A Taguchi-LHS-RSM Double-Staged Approach for Design Optimization of Self-Ventilated Cooling Systems Utilized in PMSMs

Gaojia Zhu
Power Electronics, Machines and Control Research Group
University of Nottingham
Nottingham, U.K.
zhugaojia@tiangong.edu.cn

Zeyuan Xu
Power Electronics, Machines and Control Research Group
University of Nottingham
Nottingham, U.K.
zeyuan.xu@nottingham.ac.uk

Fengyu Zhang
Power Electronics, Machines and Control Research Group
University of Nottingham
Nottingham, U.K.
fengyu.zhang1@nottingham.ac.uk

Chris Gerada
Power Electronics, Machines and Control Research Group
University of Nottingham
Nottingham, U.K.
chris.gerada@nottingham.ac.uk

David Gerada
Power Electronics, Machines and Control Research Group
University of Nottingham
Nottingham, U.K.
david.gerada@nottingham.ac.uk

***Abstract*—Thermal management is critical for high-power-density permanent magnet synchronous machines (PMSMs). To realize the efficient and effective design optimization of self-ventilated air cooling systems for PMSMs, in this paper, a Taguchi-preconditioned Latin hypercube sampling (LHS) and response surface method (RSM) combined approach is proposed. First, as the optimization variable numbers are mostly large when considering simultaneously the heat-sink and air-fan influences, the Taguchi method is employed to decouple the variables based on comprehensive fluidic-thermal calculations. The values of the less interconnected variables are optimized directly in this stage while the two most interconnected ones are selected and optimized in the next stage. Secondly, LHS is used to generate the sample points of the two variables with the values centered at the initially optimized results in the first stage. The RSM surrogate model is established with the LHS points, and the finally optimized values are then decided based on analytical analysis of the surrogate model. The proposed double-staged method is utilized in optimizing the self-ventilation system of a 2000-rpm outer rotor PMSM, and the optimization effectiveness is validated by comparing the cooling efficiency and effectiveness of the results at each optimization stage.**

Keywords—permanent magnet synchronous machine (PMSM), self-ventilated cooling system, Taguchi method, Latin hypercube sampling (LHS), response surface method (RSM)

I. INTRODUCTION

Permanent magnet synchronous machines (PMSMs) are commonly used in various industrial and transportation applications due to their superior characteristics of high efficiency, high power density, and simple dynamics [1-2]. However, when supplied with pulse width modulation (PWM) power converters, the high-frequency harmonics can generate excessive losses and therefore pose substantial challenges to machines' cooling efficiencies [3-4].

Among the existing cooling options for PMSMs, the air ventilation systems, especially in self-ventilated open-structure modes, are widely utilized as they can dissipate directly the heat generated inside the machines with very low cooling and maintenance costs [5-8]. To improve the cooling efficiency, research has been done to optimize the cooling structural parameters [9-10]. However, for air ventilation systems, as the coolant temperature varies significantly with the heating and cooling conditions, computational fluid dynamics (CFD)-based simulations are required to obtain accurately the fluidic-thermal characteristics, making the cooling system optimizations very computationally costly [11-12].

To speed up the optimization processes, the design of experiment (DoE)-based methods that can seek optimized results with limited amounts of simulations have attracted extensive research attentions [13-18]. Within those approaches, the Taguchi method, which can handle large amounts of optimization variables efficiently, has been combined with CFD calculations to optimize PMSMs' cooling systems [13-14]. The basic idea of the Taguchi method is to analyze the cooling performances with orthogonal combinations of design variables, therefore decouple those variables to find the objective versus level characteristic of each single variable [15]. However, as the variable levels in the Taguchi method are mostly very limited (≤6), the decoupling of two or more very highly interconnected variables may fail, obtaining singular relationships between the objective and the variable levels.

The Latin hypercube sampling (LHS) method can evenly distribute the variables in the solution domain with large-varying-ranged levels of each variable, thus is also commonly utilized by combining with the response surface method (RSM) to establish the surrogate models that illustrate the relationships between the cooling efficiencies and the cooling structural parameters [17-18]. But as the sampling points can get coarse when the variable number is large, the LHS-RSM method is more suitable for low-dimensional problems [19]. Since large amounts of structural variables in both the heat sinks and air fans can influence the cooling characteristics, there exists a trade-off between the optimization requirements and the merit of the LHS-RSM.

To address the aforementioned problems, in this paper, a Taguchi-preconditioned LHS-RSM-combined method is

This work was supported by the China Scholarship Council under Grant 202008120084.

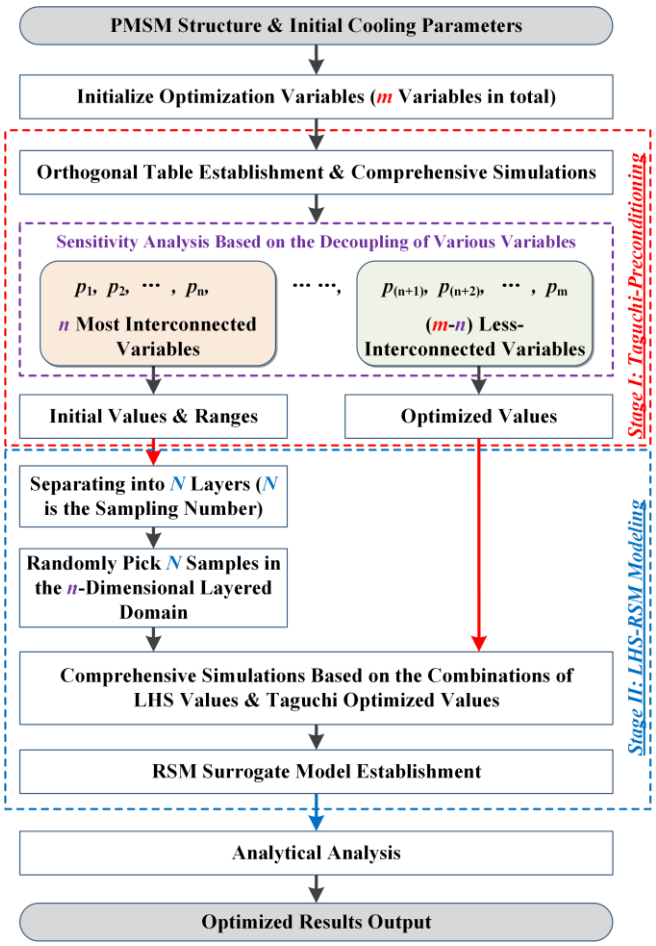

Fig. 1. The proposed Taguchi-LHS-RSM-combined optimization method.

proposed for the design optimization of the ventilation systems for PMSMs. In this approach, the overall optimization process is divided into two stages. In the first stage, the Taguchi method is combined with comprehensive CFD simulations to decouple the optimization variables. The optimized values of the less interconnected ones are determined based on the Taguchi analyses, while the two most interconnected ones are taken as the optimization variables in the next stage. Then the LHS method is used in the second stage to distribute the sampling points of the most two interconnected variables, and the RSM-based surrogate model is established depending on those sampling points. The optimized values of the two interconnected variables are then decided depending on the surrogate model. The proposed method is utilized in optimizing the self-ventilation system of a 2000-rpm outer rotor PMSM, and the fluidic-thermal characteristics of the machine with the optimized cooling structural parameters are numerically analyzed to validate the optimization effectiveness.

II. Optimization Methodology

As for the efficient and effective design optimization of air ventilation systems for PMSMs, a double-staged method with the Taguchi-based preconditioning process as the first stage and the LHS-RSM optimization process as the second stage is proposed. The overall procedure is illustrated in Fig. 1. As shown in the figure, first, the optimization variables are initially selected (m variables in total) by covering all the possible structural parameters of both the heat sink and the air fan. Then in Stage-I, the orthogonal table based on those

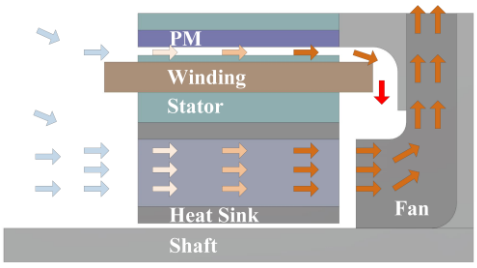

Fig. 2. Illustration on the cooling airflow of the self-ventilation system.

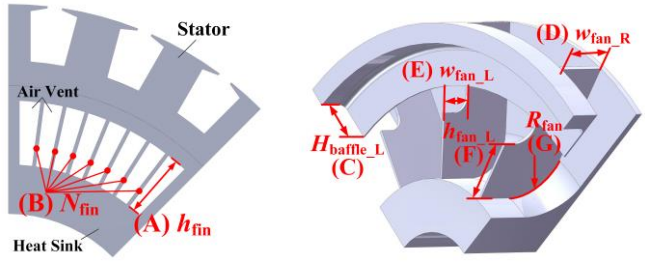

(a) (b)

Fig. 3. Illustration on initial optimization variables, where (a) variables in t heat sink, and (b) variables in the air fan.

TABLE I. Variable Levels

Variable	Level I	Level II	Level III	Level IV
(A) h_{fin}	25 mm	30 mm	35 mm	40 mm
(B) N_{fin}	5	7	9	11
(C) $h_{baffle-L}$	0 mm	8 mm	16 mm	24 mm
(D) w_{fan-R}	15 mm	20 mm	25 mm	30 mm
(E) w_{fan-L}	10 mm	12.5 mm	15 mm	17.5 mm
(F) h_{fan-L}	27 mm	37 mm	--	--
(G) R_{fan}	15 mm	25 mm	--	--

initialized variables is established. Comprehensive CFD simulations are conducted to find the fluidic-thermal coupled characteristics of each variable, and the Interconnected relations between the variables are analyzed. Among those variables, the several most interconnected ones (n variables) are selected and optimized in the next stage while the less-interconnected ones ((m-n) variables) are directly determined based on the Taguchi analysis. In Stage-II, the LHS is conducted by layering the probability domains of the selected interconnected variables into N layers (N is the sampling number) and then randomly picking N samples in the n-dimensional layered domain. It is noticed that each layer in each dimension should contain one sample point to guarantee the sampling globality. The RSM surrogate model is established based on the combinations of the sampling values and that determined by the Taguchi method in stage I. Finally, the surrogate model is analytically analyzed to obtain the optimized results.

III. Prototype and Optimization Setup

A. PMSM Prototype and Its Self-Ventilation System

To validate the effectiveness of the proposed optimization method, in this paper, a 2000-rpm self-ventilation PMSM is taken as the prototype. A centrifugal fan is mounted on the non-drive end of the shaft together with a heat sink set in the inner side of the stator core. When the fan is rotating synchronously with the shaft, the air is driven into the machine, and flows through both the air gap and the air vents in the heat sink, taking away the losses generated in the windings and the stator core, as shown in Fig. 2.

TABLE II. L16 ($4^5\times2^2$) ORTHOGONAL TABLE

ID.	(A) h_{fin}	(B) N_{fin}	(C) $h_{baffle\text{-}L}$	(D) $w_{fan\text{-}R}$	(E) $w_{fan\text{-}L}$	(F) $h_{fan\text{-}L}$	(G) R_{fan}	T_R	q_a	R_a
1	I	I	I	I	I	I	I	139.2 K	32.34 L/s	5.98 %
2	I	II	II	II	II	I	II	133.3 K	31.54 L/s	8.96 %
3	I	III	III	III	III	II	I	118.4 K	48.94 L/s	4.66 %
4	I	IV	IV	IV	IV	II	II	114.7 K	52.80 L/s	5.11 %
5	II	I	II	III	IV	I	I	118.3 K	58.93 L/s	4.13 %
6	II	II	III	IV	I	I	II	118.6 K	66.13 L/s	1.50 %
7	II	III	IV	I	II	II	I	139.7 K	36.85 L/s	0.76 %
8	II	IV	I	II	III	II	II	118.6 K	47.16 L/s	4.75 %
9	III	I	III	IV	II	I	I	116.4 K	74.08 L/s	2.54 %
10	III	II	IV	I	III	I	II	138.5 K	44.02 L/s	0.29 %
11	III	III	I	II	IV	II	I	126.5 K	53.21 L/s	0.31 %
12	III	IV	II	III	I	II	II	113.2 K	59.46 L/s	3.53 %
13	IV	I	IV	II	III	I	I	132.8 K	58.88 L/s	0.48 %
14	IV	II	I	III	IV	I	II	115.0 K	68.89 L/s	2.69 %
15	IV	III	II	IV	I	II	I	114.6 K	72.02 L/s	1.13 %
16	IV	IV	III	I	II	II	II	129.0 K	44.57 L/s	0.89 %

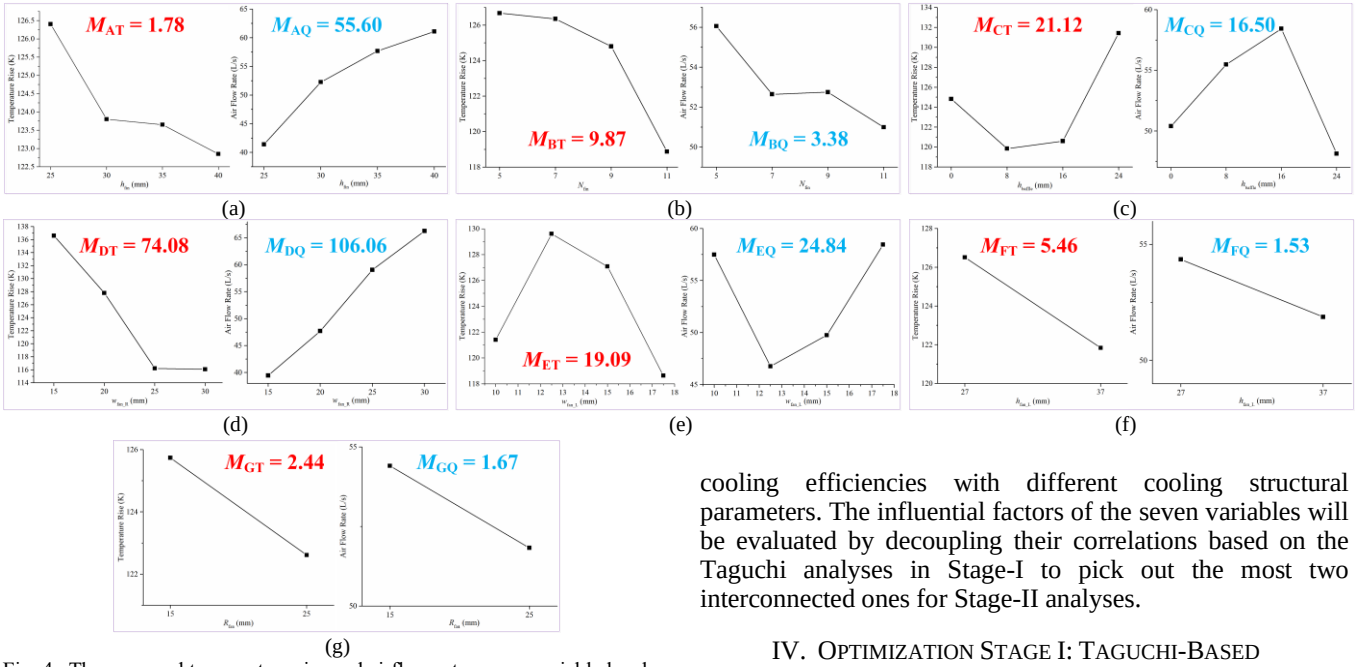

Fig. 4. The averaged temperature rise and airflow rate versus variable level, where (a) h_{fin}, (b) N_{fin}, (c) h_{baffle_L}, (d) w_{fan_R}, (e) w_{fan_L}, (f) h_{fan_L}, and (g) R_{fan}.

B. *Initial Optimization Variables and Levels*

As the structural parameters of both the heat sink and the centrifugal fan will affect simultaneously the fluidic-thermal characteristics, seven variables are selected as the initial optimization variables:

- (A) h_{fin} - Heat sink fin height.
- (B) N_{fin} - Heat sink fin number.
- (C) $h_{baffle\text{-}L}$ - Air fan baffle height (left part).
- (D) $w_{fan\text{-}R}$ - Air fan width (right part).
- (E) $w_{fan\text{-}L}$ - Air fan width (left part).
- (F) $h_{fan\text{-}L}$ - Air fan height (left part).
- (G) R_{fan} - Fillet radius of air fan baffle (right part).

The variables are illustrated in Fig. 3, with their variation levels tabulated in Table I, where the combination with all variables set at level-I is the parameters before optimization. Fluidic-thermal coupled analyses are used in obtaining the cooling efficiencies with different cooling structural parameters. The influential factors of the seven variables will be evaluated by decoupling their correlations based on the Taguchi analyses in Stage-I to pick out the most two interconnected ones for Stage-II analyses.

IV. OPTIMIZATION STAGE I: TAGUCHI-BASED PRECONDITIONING PROCESS

A. *Comprehensive Simulations and Taguchi Analysis*

Based on the initial variables and their levels (5 variables with 4 levels and 2 variables with 2 levels) selected in Section III, an L16 ($4^5\times2^2$) orthogonal table is established, as tabulated in Table II. Comprehensive fluidic-thermal calculations of the fluid flow and temperature coupled fields with the cooling structural parameters listed in the table are conducted. The calculated temperature rises (T_R), airflow rates (q_a), and the ratios of the airflow passing through the air gap (R_a) are also listed in Table II. As shown in the table, for the lines in which a certain variable is set to the same level (for example, the first 4 lines with (A) h_{fin} at level-I), the other variables will cover all possible levels, and every 2 lines are totally orthogonal to each other despite the same-leveled variable. Therefore, the approximate averaged characteristics with each variable level can be obtained, as illustrated in Fig. 4. The mean square errors of different optimization variables are computed based on the averaged values and are marked in the figure (for example, M_{AT} means the mean square error of temperature rise for the variable (A) h_{fin}, and M_{AQ} is that of airflow rate for the variable (A)).

TABLE III. INITIAL OPTIMIZED VARIABLE VALUES (WITH THE STAGE-I-DECIDED ONES MARKED BY **RED** AND THE INTERCONNECTED ONES MARKED BY **BLUE**)

Variable	① Output Result in Part 1)	② Output Result in Part 2)	③ Output Result in Stage-I
(A) h_{fin}	40 mm	35 mm	**35 mm**
(B) N_{fin}	11	--	**11**
(C) $h_{baffle\text{-}L}$	8 mm	12 mm	**12 mm**
(D) $w_{fan\text{-}R}$	25 mm	--	**25 mm**
(E) $w_{fan\text{-}L}$	17.5 mm	--	**17.5 mm**
(F) h_{fan_L}	37 mm	--	**37 mm**
(G) R_{fan}	25 mm	--	**25 mm**

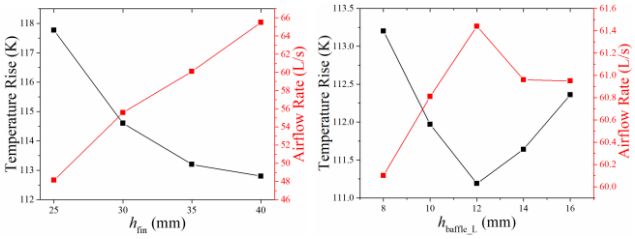

(a) (b)

Fig. 5. Temperature rise and airflow rate versus variable values in Part 2), where (a) h_{fin}, and (b) $h_{baffle\text{-}L}$.

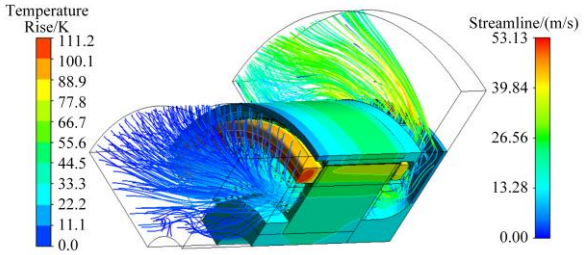

Fig. 6. Temperature rise and streamline distributions of the machine with the initially optimized parameters output in Stage-I.

B. Initial Optimized Results and Interconnected Variables

1) Variance Analysis and Variable Classification

As can be found in Fig. 5, the fan-right-part width ((D) $w_{fan\text{-}R}$) has the most significant influence on both the temperature rise and the airflow rate. The temperature rise drops with the increased $w_{fan\text{-}R}$, but the reduction rate saturates when the fan is wider than 25 mm, while the airflow rate is still climbing up. Since a larger airflow rate will cause an increased air frictional loss, (D) $w_{fan\text{-}R}$ is determined at level-III (25 mm). The fan-left-baffle height ((C) $h_{baffle\text{-}L}$) represents the second most influential behavior on the motor temperature rise, and the values at 8 mm (level-II) and 16 mm (level-III) are preferable. The reason is that, when the baffle height gets elevated, the pumping power of the air fan gets larger to generate a more significant blowing effect. However, as the higher baffle will also cause a larger flow resistance, especially to the airflow through the air gap, the baffle with the height of 24 mm (level-IV) will in turn result in the reduction of both the cooling airflow rate and the cooling effect. Since the current leveling of $h_{baffle\text{-}L}$ is relatively coarse (with doubled values (8 mm and 16 mm) between two adjacent levels), the fluidic-thermal characteristics with more levels between 8 mm and 16 mm will be comprehensively analyzed and discussed in part 2) of this section, after other parameters decided through Taguchi-based analyses.

For the other variables in the air fan, the influential factor of the fan-left-part width ((E) $w_{fan\text{-}L}$) on the temperature rise is the third largest, but the relationship is singular (the shortest and the longest ones are the preferable ones). The reason is that, when the $w_{fan\text{-}L}$ is getting larger, there will be a narrower gap between the rotating air fan and the stationary heat sink, resulting in fiercer vortexes. But when the fan-left-part width is at 17.5 mm (level-IV), the space between the air fan and the heat sink is too small to provide sufficient vortexes, and the air can flow fluently from the heat sink to the fan blades. As the aforementioned efforts are directly correlated with the fan-left-part height ((F) $h_{fan\text{-}L}$), although $h_{fan\text{-}L}$ itself represents monotonic properties with the temperature rise and the cooling airflow rate (the best at level-II, 37 mm), those two variables are strongly interconnected ones and are selected as the optimization variables in the next stage. For the fillet radius of the fan right baffle ((G) R_{fan}), as the temperature rise reduces with its increased value, the radius is decided at 25 mm (level-II).

For the heat sink parameters, the fin number ((B) N_{fin}) is preferable to be set to the largest value (level-IV, 11 fins), as the temperature rise is monotonically reduced with it due to the increased heat dissipation area. It should be mentioned that the largest cooling-fin number of 11 is restricted by the manufacturing requirements and a larger value will cause non-processable too-narrow air vents. The fin height ((A) h_{fin}) also shows monotonic characteristics with the two optimization objectives. But as the influential factor on the temperature rise is very small while that on the cooling flow rate is relatively large, fins with too large heights can only reduce the temperature slightly but caused a dramatic increase in the frictional loss. Therefore, its values will also be analyzed in part 2) of this section.

2) Further Comparisons and Initially Optimized Result

Based on the analyses in Part 1), the variables' values determined by Taguchi-based analyses are listed in the "①" row of Table III. Among those variables, (A) h_{fin} and (C) $h_{baffle\text{-}L}$ are further analyzed through comprehensive simulations in this part. For h_{fin}, with the other variables set to the ①-row values in Table III, the value varies from 25 mm to 40 mm and is further comprehensively analyzed by fluidic-thermal coupled simulations, and the comparisons of the temperature rise distributions are shown in Fig. 5(a). As can be found from the figure, the motor temperature rise reduces with the increased h_{fin}, but the reduction rate decreases when h_{fin} is larger than 35 mm. Therefore, h_{fin} is decided to be 35 mm in this part. With h_{fin} set to 35 mm, the flow-temperature coupled fields of the machine with $h_{baffle\text{-}L}$ at 8 mm, 10 mm, 12 mm, 14 mm, and 16 mm are simulated and compared, as shown in Fig. 5(b). Based on the simulation results, the 12 mm one is selected in this step. Through the comparisons between the comprehensive simulation results, the initial optimization results are determined and are listed in the "③" row of Table III, and the fluid flow and temperature rise fields with the optimized cooling structural parameters are illustrated in Fig. 6.

V. OPTIMIZATION STAGE II: LHS-RSM-COMBINED OPTIMIZATION PROCESS

A. Latin Hypercube Sampling

Based on the simulations and analyses in Stage-I, two very interconnected variables, $w_{baffle\text{-}L}$ and $h_{baffle\text{-}L}$, are taken as the optimization variables in this stage. The first step in Stage-II

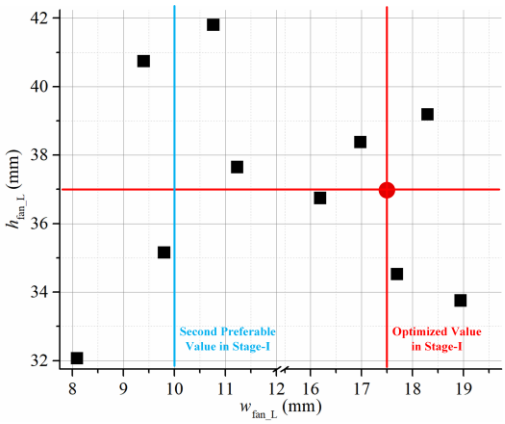

Fig. 7. LHS sampling points.

TABLE IV. FLUIDIC-THERMAL CHARACTERISTICS WITH THE SAMPLING POINTS

ID.	$w_{fan\text{-}L}$	$h_{fan\text{-}L}$	T_R	q_a
Initial	17.50 mm	37.00 mm	111.2 K	61.44 L/s
1	9.80 mm	35.16 mm	113.6 K	59.44 L/s
2	9.40 mm	40.75 mm	115.4 K	59.74 L/s
3	18.30 mm	39.19 mm	111.8 K	60.87 L/s
4	18.94 mm	33.76 mm	112.6 K	62.55 L/s
5	8.09 mm	32.07 mm	115.5 K	58.17 L/s
6	11.23 mm	37.65 mm	113.8 K	60.21 L/s
7	10.76 mm	41.80 mm	113.6 K	60.77 L/s
8	16.19 mm	36.75 mm	111.1 K	61.00 L/s
9	16.98 mm	38.38 mm	112.1 K	60.99 L/s
10	17.69 mm	34.53 mm	113.9 K	62.25 L/s

TABLE V. INTERPOLATED RSM COEFFICIENTS

Parameter	C_0	C_1	C_2
Value	127.97723	-0.67001	-0.45094
Parameter	C_3	C_4	C_5
Value	0.06165	0.01202	-0.03556

is to generate the sampling points in the ranges centered at their initial optimal values obtained in the former stage. However, it is worth noting that, for $h_{baffle\text{-}L}$, the initial optimized value occurs at 37 mm, but that for $w_{baffle\text{-}L}$ locate at two distancing sizes, 10 mm and 17.5 mm, respectively. Therefore, the ranges for sampling are selected as:

- (8.00 mm, 12.00 mm) plus (15.50 mm, 19.50 mm) for $w_{fan\text{-}L}$.
- (32.00 mm, 42.00 mm) for $h_{fan\text{-}L}$.

The LHS procedure shown in Fig. 1 is then conducted to generate the 10 sampling points, as shown in Fig. 7, where the red point illustrates the initial optimized value in Stage-I. The working performances with the sampling pointed structural parameters are also numerically investigated, and the results are tabulated in Table IV.

B. Response Surface Modeling

The 2D RSM surrogate model is employed in interpolating the relationship between the motor temperature rise and the two variables:

$$T_R\left(w_{fan\_L}, h_{fan\_L}\right) = C_0 + C_1 w_{fan\_L} + C_2 h_{fan\_L} + C_3 w_{fan\_L}^2 + C_4 h_{fan\_L}^2 + C_5 w_{fan\_L} h_{fan\_L} \quad (1)$$

TABLE VI. FINALLY OPTIMIZED RESULT OUTPUTTED

Variable	Value	T_R	q_a
(A) h_{fin}	35.00 mm	109.7 K	61.55 L/s
(B) N_{fin}	11		
(C) $h_{baffle\text{-}L}$	12.00 mm		
(D) $w_{fan\text{-}R}$	25.00 mm		
(E) $w_{fan\text{-}L}$	18.91 mm		
(F) h_{fan_L}	46.72 mm		
(G) R_{fan}	25.00 mm		

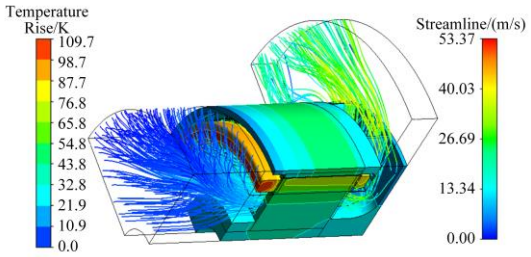

Fig. 8. Temperature rise and streamline distributions of the machine with the initially optimized parameters output in Stage-II.

where C_1, C_2, C_3, C_4, and C_5 are coefficients with their values interpolated based on the results in Table IV. The obtained coefficients are listed in Table V.

C. Finally Optimized Parameters and Comparisons

Based on the surrogate model formulated in (1), the minimum temperature rise can only occur at the stationary point of the model as:

$$\frac{\partial\left[T_R\left(w_{fan\_L}, h_{fan\_L}\right)\right]}{\partial\left(w_{fan\_L}\right)} = C_1 + 2C_3 w_{fan\_L} + C_5 h_{fan\_L} = 0 \quad (2)$$

$$\frac{\partial\left[T_R\left(w_{fan\_L}, h_{fan\_L}\right)\right]}{\partial\left(h_{fan\_L}\right)} = C_2 + 2C_4 h_{fan\_L} + C_5 w_{fan\_L} = 0 \quad (3)$$

Therefore, the stationary point is at:

$$w_{fan\_L} = \frac{2C_1C_4 - C_2C_5}{C_5^2 - 4C_3C_4} = 18.91\,(\text{mm}) \quad (4)$$

$$h_{fan\_L} = \frac{2C_2C_3 - C_1C_5}{C_5^2 - 4C_3C_4} = 46.72\,(\text{mm}) \quad (5)$$

As the second-order partial derivative can obey:

$$\frac{\partial^2\left[T_R\left(w_{fan\_L}, h_{fan\_L}\right)\right]}{\partial\left(w_{fan\_L}\right)^2}\frac{\partial^2\left[T_R\left(w_{fan\_L}, h_{fan\_L}\right)\right]}{\partial\left(h_{fan\_L}\right)^2} - \left\{\frac{\partial^2\left[T_R\left(w_{fan\_L}, h_{fan\_L}\right)\right]}{\partial\left(w_{fan\_L}\right)\partial\left(h_{fan\_L}\right)}\right\}^2 = 4C_3C_4 - C_5^2 > 0 \quad (6)$$

And:

TABLE VII. COMPARISONS BETWEEN OPTIMIZED RESULTS IN EACH STEP

Steps	Before Optimization	Part 1) of Stage-I	Part 2) of Stage-I	Output of Stage-II
T_R	139.2 K	112.8 K	111.2 K	109.7 K
Q_A	32.34 L/s	65.50 L/s	61.44 L/s	61.55 L/s

$$\frac{\partial^2\left[T_{\mathrm{R}}\left(w_{\mathrm{fan\_L}},h_{\mathrm{fan\_L}}\right)\right]}{\partial\left(w_{\mathrm{fan\_L}}\right)^2}=2C_3>0 \tag{7}$$

Therefore, the temperature rise with the cooling structural parameters at the stationary point can reach the minimum value. The final optimized cooling structural parameters are listed in Table VI, and the fluidic-thermal characteristics of the machine with the optimized ventilation structure are illustrated in Fig. 8. The machine's temperature rises at different optimization steps are compared to validate the effectiveness of the proposed methodologies, and the comparisons are listed in Table VII.

VI. CONCLUSION

In this paper, an efficient Taguchi-LHS-RSM combined method for the design optimization of self-ventilation systems for PMSMs is proposed. The method can be generally divided into two stages, in the first stage, the Taguchi method is employed with fluidic-thermal simulations to determine the initially optimized values of the cooling structural variables, and the most interconnected variables are selected and utilized in the next stage. In Stage-II, the LHS points are generated with the interconnected variable space centered at the initially optimized values in Stage-I. The RSM surrogate model is then established based on the LHS points with the fluid flow and thermal characteristics analyzed through CFD simulations. The final optimized values are obtained based on the analytical analysis of the RSM model. The proposed method is employed in finding the optimal design of the self-ventilation system for an outer rotor PMSM prototype, and the effectiveness of the methodology is validated by comparing the results at different optimization stages.

REFERENCES

[1] Y. G. Chen, B. Q. Zang, H. T. Wang, H. X. Liu, and H. R. Li, "Composite PM rotor design and alternating flux density harmonic component analysis of a 200 kW high-speed PMSM used in FESS," IEEE Trans. Ind. Appl., vol. 59, no. 2, pp. 1469-1480, March/April 2023.

[2] H. Chen, N. A. O. Demerdash, A. M. EL-Refaie, Y. G. Guo, W. Hua, and C. H. T. Lee, "Investigation of a 3D-magnetic flux PMSM with high torque density for electric vehicles," IEEE Trans. Energy Conver., vol. 37, no. 2, pp. 1442-1454, June 2022.

[3] N. Z. Popov, S. N. Vukosavic, and E. Levi, "Motor temperature monitoring based on impedance estimation at PWM frequencies," IEEE Trans. Energy Conver., vol. 29, no. 1, pp. 215-223, March 2014.

[4] X. D. Sun, B. K. Wan, G. Lei, X. Tian, Y. G. Guo, and J. G. Zhu, "Multiobjective and multiphysics design optimization of a switched reluctance motor for electric vehicle applications," IEEE Trans. Energy Conver., vol. 36, no. 4, pp. 3294-3304, December 2021.

[5] Y. C. Chong, E. J. P. E. Subiabre, M. A. Mueller, J. Chick, D. A. Staton, and A. S. McDonald, "The ventilation effect on stator convective heat transfer of an axial-flux permanent-magnet machine," IEEE Trans. Ind. Electron., vol. 61, no. 8, pp. 4392-4403, August 2014.

[6] M. Kondo, Y. Shimizu, and J. Kawamura, "Development of totally enclosed permanent magnet synchronous motor," Q. Rep. RTRI, vol. 49, no. 1, pp. 16-19, February 2008.

[7] W. L. Li, Z. B. Cao, and X. C. Zhang, "Thermal analysis of the solid rotor permanent magnet synchronous motors with air-cooled hybrid ventilation systems," IEEE Trans. Ind. Electron., vol. 69, no. 2, pp. 1146-1156, February 2022.

[8] L. K. Wang, Y. Li, F. Marignetti, and A. Boglietti, "Coupled fluid-solid heat transfer of a gas and liquid cooling PMSM including rotor rotation," IEEE Trans. Energy Conver., vol. 37, no. 1, pp. 443-453, March 2022.

[9] A. Tüysüz, F. Meyer, M. Steichen, C. Zwyssig, and J. W. Kolar, "Advanced cooling methods for high-speed electrical machines," IEEE Trans. Ind. Appl., vol. 53, no. 3, pp. 2077-2087, May/June 2017.

[10] J. Buschbeck, M. Vogelsberger, A. Orellano, and E. Schmidt, "Pareto optimization in terms of electromagnetic and thermal characteristics of air-cooled asynchronous induction machines applied in railway traction drives," IEEE Trans. Magn., vol. 52, no. 3, March 2016, Art. no. 8101004.

[11] A. Boglietti, A. Cavagnino, D. Staton, M. Shanel, M. Mueller, and C. Mejuto, "Evolution and modern approaches for thermal analysis of electrical machines," IEEE Trans. Ind. Electron., vol. 56, no. 3, pp. 871-882, February 2009.

[12] S. J. Wakes, B. O. Bauer, and M. Mayo, "A preliminary assessment of machine learning algorithms for predicting CFD-simulated wind flow patterns over idealised foredunes," J. R. Soc. N.Z., vol. 51, no. 2, pp. 290-306, April 2021.

[13] L. N. Li, N. Jia, X. Z. Wang, Y. R. Yun, and G. J. Zhu, "Cooling system design optimization of an enclosed PM traction motor for subway propulsion systems," CES Trans. Elet. Mach. Syst., in press.

[14] G. J. Zhu, L. N. Li, Y. H. Mei, T. Liu, and M. Xue, "Design and analysis of a self-circulated oil cooling system enclosed in hollow shafts for axial-flux PMSMs," IEEE Trans. Veh. Technol., vol. 71, no. 5, pp. 4879-4888, May 2022.

[15] Z. Shi, X. D. Sun, Y. F. Cai, and Z. B. Yang, "Robust design optimization of a five-phase PM hub motor for fault-tolerant operation based on Taguchi method," IEEE Trans. Energy Convers., vol. 35, no. 4, pp. 2036-2044. December 2020.

[16] X. D. Sun, Z. Shi, and J. G. Zhu, "Multiobjective design optimization of an IPMSM for EVs based on fuzzy method and sequential Taguchi method," IEEE Trans. Ind. Electron., vol. 68, no. 11, pp. 10592-10600, November 2021.

[17] D. K. Hong, D. Joo, J. Y. Lee, B. C. Woo, K. S. Kim, and J. P. Hong, "Development of a large diameter motor for turret application," IEEE Trans. Magn., vol. 49, no. 5, pp. 2327-2330, May 2013.

[18] Y. S. Li, C. B. Li, A. Garg, L. Gao, and W. Li, "Heat dissipation analysis and multi-objective optimization of a permanent magnet synchronous motor using surrogate assisted method," Case Stud. Therm. Eng., vol. 27, October 2021, Art. no. 101203.

[19] X. J. Zhou, D. K. J. Lin, X. L. Hu, and L. H. Ouyang, "Sequential latin hypercube design with both space-filling and projective properties," Qual. Reliab. Eng. Int., vol. 35, pp. 1941-1951, October 2019.